Probing the reactivity of different forms of azurin by flavin photoreduction

Alagarathnam, S.; Meeuwenoord, N.J.; Navarro, J.A.; Hervás, M.; Rosa, M.A. de la; Hoffmann, M.; ... ; Canters, G.W.

the FEBS Journal

Probing the reactivity of different forms of azurin by flavin photoreduction

Sharmini Alagaratnam[1], Nico J. Meeuwenoord[1], José A. Navarro[2], Manuel Hervás[2], Miguel A. De la Rosa[2], Maren Hoffmann[3], Oliver Einsle[3], Marcellus Ubbink[1] and Gerard W. Canters[1,4]

1 Gorlaeus Laboratories, Leiden Institute of Chemistry, Leiden University, The Netherlands
2 Instituto de Bioquímica Vegetal y Fotosíntesis, Universidad de Sevilla y CSIC, Sevilla, Spain
3 Institute of Organic Chemistry & Biochemistry, Albert Ludwigs University, Freiburg, Germany
4 Huygens Laboratory, Leiden Inistitute of Physics, Leiden University, The Netherlands

Keywords
Cu protein; electron transfer; flash photolysis; flavin; protein cavity

Correspondence
G. W. Canters, Gorlaeus Laboratories, Leiden University, Einsteinweg 55, 2333 CC, Leiden, The Netherlands
Fax: +31 71 527 4349
Tel: +31 71 527 4256
E-mail: canters@chem.leidenuniv.nl

(Received 20 November 2010, accepted 24 February 2011)

doi:10.1111/j.1742-4658.2011.08067.x

The reactivity of a variant of the blue copper protein, azurin from *Pseudomonas aeruginosa*, was investigated with laser flash photolysis and compared with the reactivity of the wild-type (WT) protein. The variant was obtained by changing the Cu ligating His117 for a glycine. The mutation creates a gap in the ligand shell of the Cu that can be filled with external ligands or water molecules. The crystal structure of the H117G variant is reported. It shows that the immediate surrounding of the Cu site in the variant exhibits less rigidity than in the WT protein and that the loop containing the Cu ligands Cys112, His117 and Met121 in the WT protein has gained flexibility in the H117G variant. Flash photolysis experiments were performed with 5-deazariboflavin and 8α-imidazolyl-(*N*-propylyl)-amino riboflavin as electron donors to probe the reactivity of WT and H117G azurin, and of H117G azurin for which the gap in the Cu co-ordination shell was filled with imidazole. 8α-Imidazolyl-(*N*-propylyl)-amino riboflavin appears one to two orders less efficient as a photo-flash reductant than 5-deazariboflavin. The reactivity of the H117G variant in the absence of external ligands appears to be 2.5-fold lower than the WT reactivity (second-order rate constants of $51 \pm 2 \times 10^7$ $M^{-1}s^{-1}$ versus $21 \pm 1 \times 10^7$ $M^{-1}s^{-1}$), whereas the addition of imidazole restores reactivity to above the WT level ($71 \pm 4 \times 10^7$ $M^{-1}s^{-1}$). The differences are discussed in terms of structural modifications and changes in reorganizational energy and electronic coupling.

Database
Structural data are available in the Protein Data Bank under the accession number 3N2J.

Structured digital abstract
• Azurin binds to Azurin by x-ray crystallography (View interaction)

Introduction

There is continuing interest in the effect of modifications of proteins (in particular enzymes) on their reactivity. The interest arises not only from a fundamental point of view, but also because of possible applications

Abbreviations
5-dRf, 5-deazariboflavin; 4-EPMH, 4-ethylphenol methylene hydroxylase; ET, electron transfer; Im-Cu-H117G azurin, imidazole bound to Cu-H117G azurin; IPAR, 8α-imidazolyl-(*N*-propylyl)-amino riboflavin; PDB, Protein Data Bank; WT, wild-type.

in industrial processes and nanobiotechnology. A relevant type of modification relates to changes in the active site of an enzyme that are brought about by taking out the prosthetic group and filling the gap with a group that slightly differs from the original. In this way, the mechanistic properties of the enzyme may be manipulated. Examples include the incorporation of metals into an active site [1–3] or the replacement of prosthetic haem [4–7] and flavin [8–10] groups by their modified equivalents.

A particularly interesting case is provided by metal-containing active sites in which the metal is held in place by side chains of amino acids. By replacing one of the ligating residues for a glycine or an alanine, a gap is created in the ligand shell that may be filled by an external ligand [11]. When the ligand is attached to a linker, in principle, easy and direct access is obtained to the catalytic heart of the protein. This approach has been employed to create a photoexcitable myoglobin in which a ruthenium group had been covalently attached to the protein's haem cofactor [12].

It is important to know how such a modification may affect the activity of the protein. We aimed to investigate this question by focusing on a blue copper protein. It is possible to modify the active site of the electron transfer (ET) protein azurin from *Pseudomonas aeruginosa* so that it becomes accessible from the outside. In the wild-type (WT) protein, a copper ion is held in place by three strongly co-ordinating almost co-planar ligands, Cys112 and His46 and His117, plus a weaker distal ligand, Met121, together forming a so-called type-1 copper site [13,14]. Exchanging the surface-exposed His117 ligand for a nonco-ordinating glycine (Cu-H117G azurin) creates a cavity by which the copper becomes accessible to external ligands [15]. In the absence of such ligands, water molecules fill the gap [16,17], giving rise to a geometry more typical of a type-2 copper site [18]. Binding of imidazole to Cu-H117G azurin (Im-Cu-H117G azurin) was found to restore the spectroscopic features of the copper site of the WT species [15].

Three of the above mentioned residues (i.e. Cys112, His117 and Met121) are located on a single loop. It has been shown by Sato *et al.* [19] that the 3D-structure of the loop is dictated by the length of the amino acid stretches between Cys112 and His117 and between His117 and Met121, and is independent of the nature of the intervening amino acid residues, whereas the Cu binding residues serve as anchoring points for the loop. It is therefore of interest to determine the structure of the loop when the central anchoring point (His117) has been abolished. Crystallographic data are reported on crystals of the oxidized Cu-H117G species. The structure shows an exceptionally exposed copper site with only loosely associated water molecules [16–18].

The mechanistic properties of a blue copper protein depend among others on the midpoint potential (E_0) of the Cu site and the ability to form complexes with redox partners. As Marshall *et al.* [20] have reported, factors such as hydrophobicity of the Cu binding residues, the presence of electrostatic dipoles in the vicinity of the Cu, and the H-bridge pattern involving the Cys112 Sγ atom have a decisive influence on the midpoint potential of the Cu site. It is therefore not unexpected that the replacement of His117 by a glycine causes a pronounced change in the midpoint potential: E_0 increases to 670 mV [21]. This has been ascribed to the freedom, resulting from the mutation, for the Cu to adopt a 3- instead of a 4-co-ordinated geometry [17,21]. As a 3-co-ordination strongly favours the Cu(I) state over the Cu(II) state, this explains the rise in midpoint potential. A similar type of reasoning explains the unusually high midpoint potential of the C112D/M121E variant of azurin from *P. aeruginosa* where structural constraints force the Cu site to adopt a 3-co-ordinate structure at low pH [22].

The other parameter relates to the ability of the protein to form complexes with redox partners. Because ET occurs through His117, the formation of an ET-competent association complex with a redox partner depends to a large extent on the details of the surface patch surrounding His117. The placement of His117 in the middle of a loop offers an ideal structural motif to tune the surface characteristics by varying the loop residues, at the same time as maintaining the structure of the loop by fixing the anchoring points and the lengths of the loop fragments in between the anchoring points, thereby preserving the capability of His117 to function as the ET conduit to the Cu site [19,23]. In light of the structural details reported, it is of interest to investigate the activity of the H117G variant in the presence and absence of different external analogues of the His side chain.

In the present study, we have used flavin-mediated laser flash photolysis to probe the reactivity of the Cu-H117G and Im-Cu-H117G azurin variants and to compare them with WT azurin [24]. As reductants, two different flavins were used: 5-deazariboflavin (5-dRf) and 8α-imidazolyl-N-propylyl-amino-riboflavin (IPAR) (Fig. 1). The midpoint potential of the quinone/semiquinone couple of 5-dRf is −650 mV [25], which makes 5-dRf$^{-\bullet}$ a powerful electron donor. IPAR, on the other hand, can be used not only as an alternative electron donor, but also for insertion into

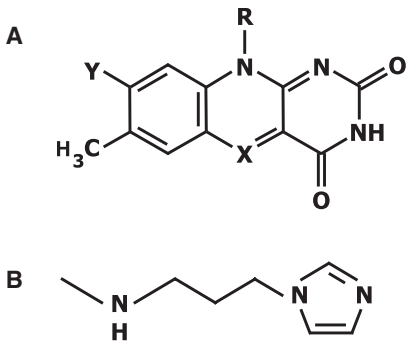

Fig. 1. (A) General structure of flavins where Y is the 8α position and R = ribityl chain. (B) In 5-deazariboflavin: X = C and Y = CH_3. In IPAR: X = N and Y = 1-(3-aminopropyl)-imidazole.

H117G azurin. Because, in the latter case, the photoexcitable moiety (i.e. the riboflavin) is covalently attached to the imidazole that inserts into the Cu site, in principle, it offers the possibility to study the process of intramolecular electron transfer along an engineered linker. The reactivities of WT, Im-Cu H117G and Cu-H117G azurin towards reduction by 5-dRf$^{-\bullet}$ and IPAR are reported and compared, and the reasons for the significant difference in reactivity between the two reductants are discussed.

Results

IPAR synthesis and characterization

Synthesis

The synthetic route for IPAR is shown in Fig. 2. The four hydroxyl groups on the ribityl side chain of riboflavin (**1**) were first protected by acetylation giving tetra-acetyl riboflavin (**2**). The 8α position of this molecule was then brominated to give 8α-bromo-tetra-acetyl-riboflavin (**3**). Subsequently, this compound was substituted with 1-(3-aminopropyl)-imidazole (**4**) before deacetylation to give the final product IPAR (**5**). ^{1}H-NMR and MS confirmed the identity of the molecule.

ε_{445} of IPAR

The electronic absorption spectrum of IPAR was found to be very similar to that of its precursor riboflavin (Fig. 3) with one significant difference, namely a blue shift of approximately 20 nm of the near UV flavin absorption band to 350 nm. The extinction coefficient of IPAR at 445 nm, determined as described in the Materials and methods, amounted to 13.0 ± 0.3 $mM^{-1}\cdot cm^{-1}$.

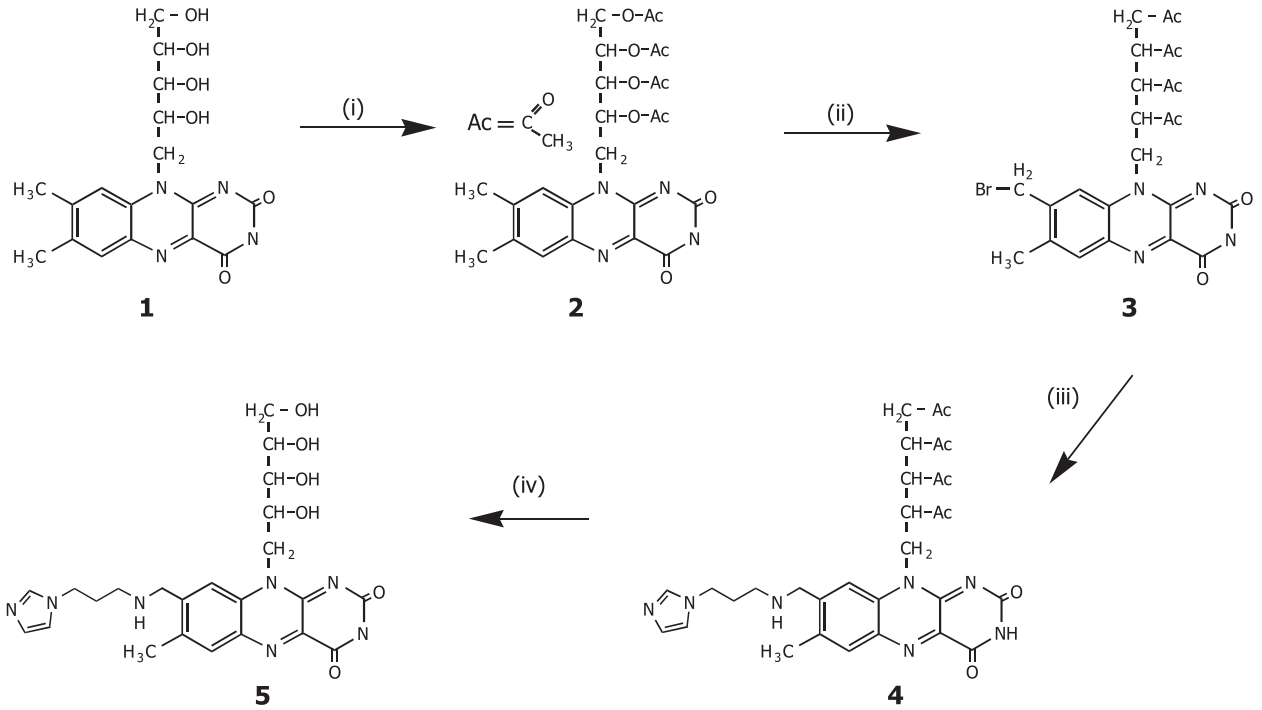

Fig. 2. Synthetic route for IPAR: (i) flavin peracetylation; (ii) 8α-monobromination; (iii) substitution of bromine with 1-(3-aminopropyl)-imidazole; (iv) deacetylation of ribityl sidechain.

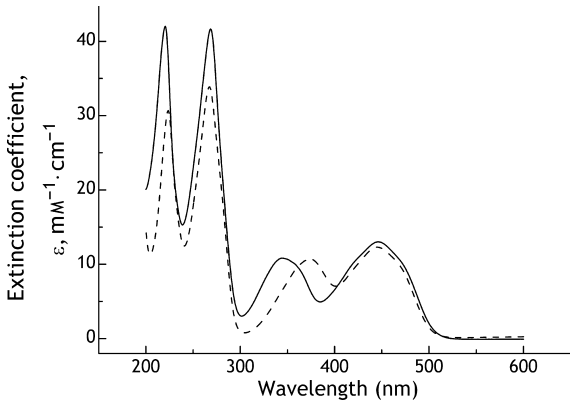

Fig. 3. UV-visible spectra of oxidized solutions of IPAR (solid line) and riboflavin (dashed line), in water at 25 °C.

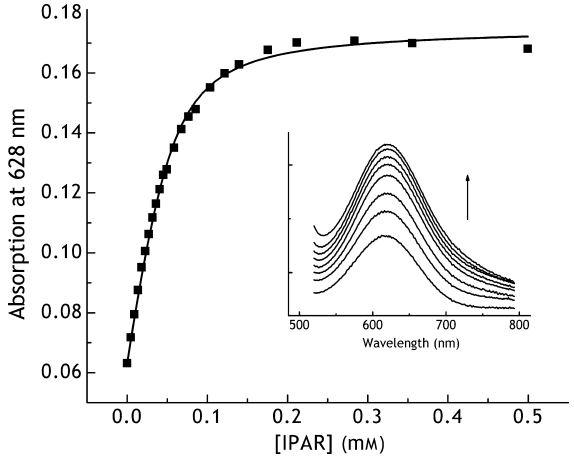

Fig. 4. The absorption at 628 nm (black squares) of a 45 μM aqueous solution of Cu-H117G azurin (in 20 mM Mes, pH 6.0, 25 °C) as a function of IPAR concentration, was fitted (solid line) as described previously [17], yielding a K_d^{app} of 12 ± 1 μM. Inset: visible spectra of Cu-H117G azurin with increasing concentrations of IPAR (0, 18, 37, 59, 95, 124, 176 and 220 μM). The arrow indicates the direction of the changes observed with increasing concentrations of IPAR.

K_d of IPAR-Cu-H117G

Figure 4 shows the increase in A_{628} upon the addition of IPAR to Cu-H117G azurin at pH 6.0, from which the apparent dissociation constant (K_d^{app}) for IPAR binding to Cu-H117G azurin could be determined using the fitting procedure described previously [17]. The K_d^{app} thus obtained was 12 ± 1 μM, and correcting for imidazolyl protonation (pK_a = 7.0) gave K_d = 1.1 ± 0.1 μM.

E_m of IPAR

Addition of aliquots of dithionite to the IPAR solution led to the gradual loss of absorption at 445 nm, with

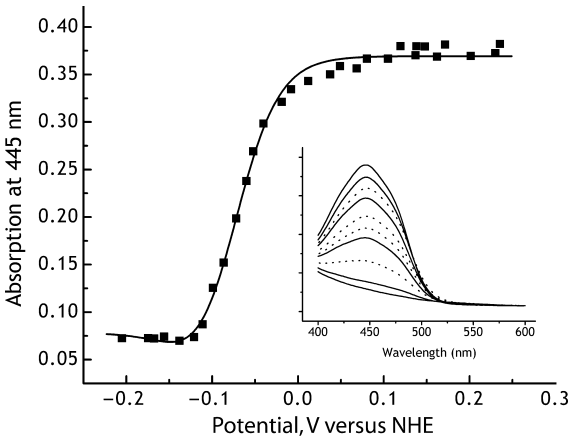

Fig. 5. Potentiometric titration of 30 μM of IPAR in 20 mM Mes (pH 6.0), 25 °C, fitting the absorbance changes upon oxidation and reduction at 445 nm as described in the Materials and methods. Inset: absorbance spectra showing the changes in going from the quinone to the hydroquinone and back to the quinone form of IPAR, solid lines are curves from the reductive titration, and dotted lines from the oxidative titration.

no other absorption changes in the range 400–800 nm. Reoxidation of the solution by the addition of ferricyanide resulted in recovery of the 445 nm peak. These changes, shown in Fig. 5, indicate that IPAR undergoes two-electron reduction to its hydroquinone form, as has previously been observed for other flavins free in solution [26,27]. Fitting of changes in A_{445} (Fig. 5), as described in the Materials and methods, showed that the fit was rather insensitive to ε_{445}^{sq}, leading to a large uncertainty in this value. As a result, only approximate values for the midpoint potentials could be determined, with E_m (the two-electron redox potential of IPAR) = −71 ± 7 mV, and E_1 and E_2 within 40 mV on either side of this value.

Laser flash photolysis

Laser flash photolysis of a mixture of 5-dRf and Im-Cu-H117G azurin in 20 mM Mes buffer at pH 6.0 gave rise to kinetic transients as shown in Fig. 6. At 520 nm, where the 5-dRf semiquinone radical absorbs maximally, an initial rise in absorbance is followed by a slower decay. This decay is concurrent with the decay in absorbance observed at 630 nm, where the reduction of copper in azurin is followed. Consequently, similar kinetic rate constants were estimated at both wavelengths (not shown). This behaviour was observed for 5-dRf in combination with WT azurin, Im-Cu-H117G and Cu-H117G, as well as for IPAR in combination with WT azurin and Im-Cu-H117G. The rate of flavin semiquinone decay, concurrent with copper reduction,

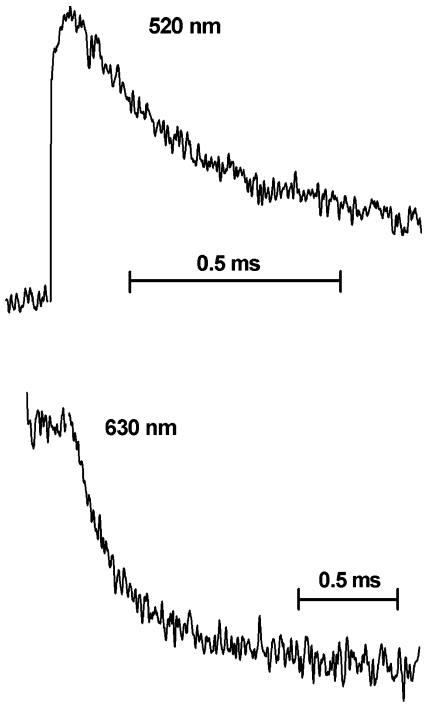

Fig. 6. Transient absorbance changes showing the rapid formation then further slow decay of 5-dRf semiquinone radical measured at 520 nm (top trace), and reduction of Cu(II) Im-Cu-H117G azurin measured at 630 nm (bottom trace). The concentration of Im-Cu-H117G azurin was 25 μM, in 20 mM Mes (pH 6.0) and 100 μM 5-dRf at room temperature. Grey lines correspond to the theoretical fits according to monoexponential decays.

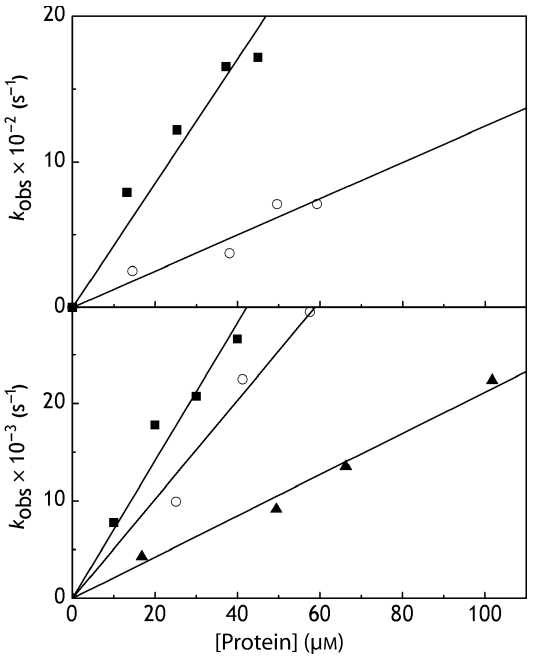

Fig. 7. Dependence of observed rates (k_{obs}) for reduction of different azurin species under pseudo first-order conditions by 5-dRf (lower plot) and IPAR (upper plot) semiquinone radicals on concentration of WT (open circles), Im-Cu-H117G azurin (solid squares) and Cu-H117G (solid triangles) azurin. For experimental details, see Materials and methods.

increased linearly with the concentration of all species of oxidized copper azurin tested. Plotting the observed rates against oxidized protein concentration (Fig. 7) allowed the determination of the second-order rate constant, k_2, as summarized in Table 1.

To obtain k_2 for the combination of IPAR with IPAR-Cu-H117G, increasing and equimolar amounts of IPAR and Cu-H117G were subjected to laser flash photolysis in 20 mM Mes (pH 6.0) using IPAR as the sole electron donor. Again, rates of azurin reduction varied linearly with protein concentration (Fig. 8). With the concentrations of protein and IPAR used for the experiment, the solution contains an approximately equimolar mixture of Cu-H117G and IPAR-Cu-H117G. Because the main absorption band of Cu-H117G occurs at 420 nm [18,21], the change in A_{630} monitored in the experiment is almost exclusively a result of the reduction of IPAR-Cu-H117G. Therefore, no k_2 value could be determined for the combination IPAR/Cu-H117G and only the second-order rate constant for the combination IPAR/IPAR-Cu-H117G corrected for the dissocition equilibrium is quoted in Table 1.

Table 1. Second-order rate constants, k_2, for azurin reduction obtained for different azurin species with 5-dRf and IPAR as electron donors. ND, not determined.

	k_2 ($\times 10^7$ $M^{-1}{\cdot}s^{-1}$)	
Azurin species	5-dRf	IPAR
WT	51 ± 2	1.1 ± 0.1
Cu-H117G	21 ± 1	ND
Im-Cu-H117G	71 ± 4	4.3 ± 0.3
IPAR-Cu-H117G	ND	3.4 ± 0.5

Crystal structure of Cu-H117G azurin

The structure of the copper-bound form of H117G azurin in the absence of other external ligands was solved by X-ray crystallography to a resolution of 1.35 Å. A total of twelve Cu-co-ordinated H117G molecules were located in the asymmetric unit of the $P2_1$ unit cell. The entire core of the protein was fully maintained, as indicated by rmsd of the positions of all C_α atoms from those of WT azurin [Protein Data Bank (PDB) code: 4AZU] [14] in the range 0.21–0.38 Å. The H117G mutation resulted in the loss of a crucial attachment point to the protein core for the

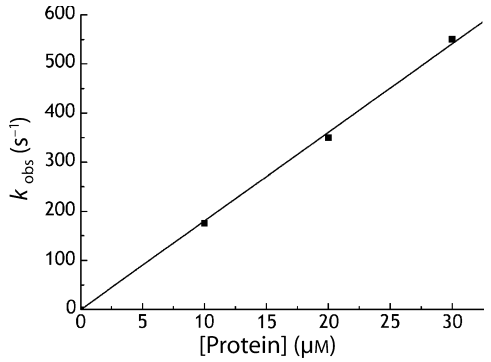

Fig. 8. Rate of reduction (k_{obs}) of IPAR-Cu-H117G by IPAR semiquinone radicals as a function of protein concentration. Total IPAR concentration was kept equal to the total protein concentration.

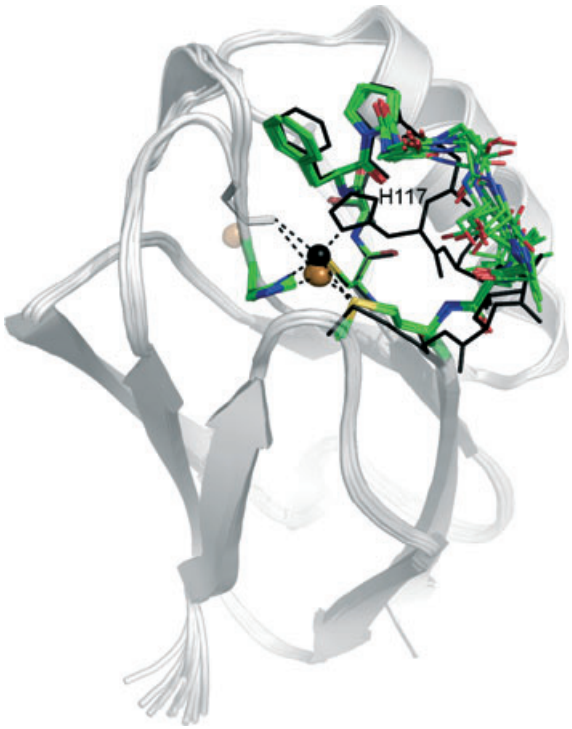

Fig. 9. Superposition of the twelve monomers of azurin Cu-H117G observed in the asymmetric unit of the $P2_1$ cell. The conformation of the ligand loop in the WT protein is shown in black, the loops of the mutant monomers are coloured by atom type.

metal-binding loop (Fig. 9). This loop subsequently adopted a less rigid conformation in all monomers, which was clearly different from that observed in WT azurin, emphasizing that the effect of the mutation is larger than merely opening up a free co-ordination site on the copper ion.

To determine the identity of the metal ion in H117G azurin, anomalous double difference maps were calculated from two data sets collected at energies immediately below and above the copper K-edge at 8979 eV (λ = 1.3808 Å). Difference peaks observed in such maps allow for the unambiguous identification of an element and, in the H117G structure, their presence clearly indicated a copper ion not only in the metal-binding site, but also at a second position, co-ordinated to the $N_{\varepsilon 2}$ of His83 (data not shown). In the latter position, the metal ion was involved in various intermolecular contacts within the crystal lattice, making it a putative factor for crystal formation. A similar role for Zn ions has been reported by Crowley *et al.* [28] for the case of plastocyanin.

Because of the the absence of His117 as a ligand, the copper site in the mutant is much more solvent exposed than in WT azurin. In all monomers, water has been modelled as a ligand to the copper, albeit in slightly varying positions that reflect the high degree of conformational flexibility in and around the metal-binding loop. Nevertheless, the geometry of the copper ligation by the remaining His46, Cys112 and Met121 is consistent in all monomers. It differs markedly from the canonical type-I copper geometry observed in WT azurin that is commonly described as trigonal bipyramidal, with the copper ion located almost in the plane of His46, Cys112 and His117, with Met121 and the backbone carbonyl of Gly45 serving as axial ligands. In the H117G mutant, by contrast, the copper has moved into the plane of the remaining ligands, His46, Cys112 and Met121 (Fig. 10), with significantly altered bond distances (Table 2). In general, both the Cu–S_γCys112 and Cu–$N_{\delta 1}$His46 distances are decreased by approximately 0.1 Å, whereas the Cu–S_δMet121 distance is even decreased by approximately 0.5 Å. At the same time, the interaction with the backbone carbonyl of Gly45 is weakened and its bond distance increased by 0.4 Å.

Discussion

Optical spectra

The new flavin derivative IPAR was found to have characteristics comparable to other similarly substituted riboflavins. The shift of the near UV absorption band of IPAR as a result of the presence of the 1-(3-aminopropyl)-imidazole group, is similar in character and magnitude to shifts that have been observed upon substitution at the 8α-position of riboflavin and FMN with histidine [29] as well as imidazole groups [30,31]. The ε_{445} for IPAR is a little higher than for the parent compound, although not significantly different from other flavins, both substituted and nonsubstituted [30].

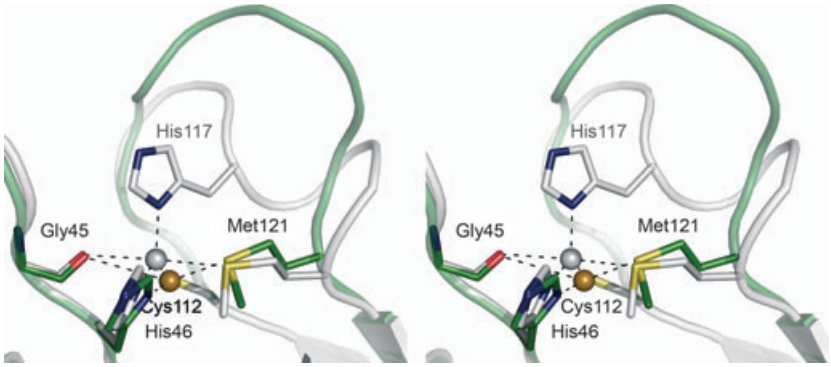

Fig. 10. Superposition (in stereo) of the surrounding of the copper site in WT azurin (grey) and in the Cu-H117G mutant (green), emphasizing the relative displacement of the Cu^{2+} ion and of the ligand-binding loop in the absence of the co-ordinating histidine.

Table 2. Bond distances (Å) at the copper site in Cu-H117G compared to the four monomers of WT azurin (PDB code: 4AZU).

	Cu–N^{δ}His46	Cu–S^{γ}Cys112	Cu–N^{δ}His117	Cu–S^{δ}Met221	Cu–OGly45
Azurin H117G					
A	2.00	2.12	–	2.51	3.50
B	2.00	2.13	–	2.65	3.45
C	1.98	2.06	–	2.73	3.38
D	1.97	2.07	–	2.70	3.40
E	2.00	2.10	–	2.53	3.48
F	1.98	2.09	–	2.58	3.34
G	1.97	2.09	–	2.56	3.34
H	1.94	2.18	–	2.54	3.44
I	1.96	2.01	–	2.83	3.39
J	1.91	2.08	–	2.58	3.33
K	2.02	2.16	–	2.58	3.35
L	1.94	2.10	–	2.62	3.40
Mean	1.97 ± 0.03	2.10 ± 0.04	–	2.62 ± 0.10	3.40 ± 0.06
WT azurin (4AZU)					
A	1.99	2.27	2.11	3.18	2.84
B	2.06	2.27	1.98	3.16	2.95
C	2.13	2.24	1.96	3.21	3.05
D	2.12	2.17	2.00	3.05	3.03
Mean	2.08 ± 0.07	2.24 ± 0.05	2.01 ± 0.07	3.15 ± 0.07	2.97 ± 0.10

IPAR binding to H117G azurin

K_d. After the increase of the blue absorption band at 628 nm with addition of IPAR to Cu-H117G azurin appeared to comprise a suitable method for estimation of the K_d^{app} for IPAR binding to Cu-H117G azurin (K_d^{app} = 12 μM at pH 6.0, K_d = 1.1 ± 0.1 μM). The concurrent decrease of the absorption band at 420 nm could not be observed because the intense IPAR absorption peaks obscure the azurin spectrum in this region. Crucially, restoration of Cu-H117G to the spectroscopic features of the WT protein strongly indicates the structural restoration of the mutated site by the addition of the IPAR ligand. The dissociation constant of 1.1 μM for the binding of IPAR to Cu-H117G is slightly lower than that for the binding of imidazole, 2.4 μM [17]. This indicates that neither the linker, nor the flavin parts of IPAR adversely affect the binding of the imidazole moiety to the mutated copper site. Indeed, partial burying of the alkyl moiety of IPAR within the protein may lead to an overall positive entropic effect.

Redox characteristics of IPAR

Redox titration curves for flavins have long been known to deviate from that predicted by the Nernst equation for the transfer of two electrons as a result of the presence of the semiquinone intermediate [32]. A modified equation taking this into account fits

the redox potentiometric data much better [33]. At −71 mV, the E_m obtained for IPAR is 90 mV higher than that of riboflavin (−161 mV) [27] but closer to that of 8α-*N*-imidazole substituted riboflavin (−104.5 mV) [26] (all values at pH 6.0). Furthermore, it is immediately obvious that the E_m of IPAR (−71 mV) is substantially higher than that of 5-dRf (−320 mV) [25] by almost 250 mV, as might be expected because it resembles its riboflavin precursor more than the deaza analogue. Similarly, it may be assumed that the midpoint potential of the ox/sq couple is substantially more positive for IPAR than for 5-dRf.

Laser flash photolysis

5-dRf versus IPAR as reductant

The transient absorbance changes observed in Fig. 6 with 5-dRf as the reductant are consistent with the rapid formation of flavin semiquinone radical, in line with the idea that the MES buffer plays a role as a sacrificial electron donor analogous to EDTA [34,35]. The second-order rate constants obtained for 5-dRf/MES (Table 1) are within the same order of magnitude as those obtained using riboflavin/EDTA to reduce plastocyanin (1.5×10^9 M^{-1}·s^{-1}) [36], indicating that oxidation of Mes by triplet flavin occurs efficiently. IPAR also proved to be viable as an electron donor, albeit with second-order rate constants that were approximately one to two orders of magnitude lower than with 5-dRf (Table 1). This may be related to the more negative ox/sq midpoint potential of 5-dRf compared to IPAR, leading to a larger driving force for the ET reaction. A semi-empirical equation for the exponential decay of the electron tunnelling rate k_{et} for non-adiabatic electron transfer [37],

$$\log k_{et} = 15 - 0.6R - 3.1(\Delta G + \lambda)^2/\lambda$$

where R is the edge-to-edge distance between the redox centres in Å, λ is the reorganization energy in electron volts, and ΔG is the driving force for the reaction in electron volts, predicts higher rates of electron transfer with larger $|\Delta G|$, provided that $|\Delta G| < \lambda$. A difference of 0.5 eV between IPAR and 5-dRf could easily lead to an order of magnitude difference in rate constants.

Laser flash photolysis: Im-Cu-H117G, Cu-H117G and Im-Cu-H117G as electron acceptors

With both electron donors, Im-Cu-H117G azurin is reduced with higher second-order rate constants than WT azurin ($71 \pm 4 \times 10^7$ M^{-1}·s^{-1} versus $51 \pm 2 \times 10^7$ M^{-1}·s^{-1} and $4.3 \pm 0.3 \times 10^7$ M^{-1}·s^{-1} versus $1.8 \pm 0.3 \times 10^7$ M^{-1}·s^{-1} for 5-dRf and IPAR, respectively). Two points are worthy of note. First, the present finding is contrary to what has been observed previously for the reduction of these two azurin species by the enzyme 4-ethylphenol methylene hydroxylase (4-EPMH), where Im-Cu-H117G was reduced at a rate of one order of magnitude lower than WT azurin [38]. The contrasting behaviour of 5-dRf and IPAR compared to 4-EPMH may reflect differences between the large 4-EPMH enzyme and the much smaller 5-dRf and IPAR molecules in the efficiency of productive complex formation. Second, the higher reactivity of Im-Cu-H117G over the WT protein should be considered in relation to the dynamics that accompany the reduction of the Cu site in Im-Cu-H117G azurin. It has been reported [15,17,21] that reduction of the Cu site is accompanied by dissociation of the imidazole. This constitutes a significant change in the co-ordination geometry of the copper (from 4- to 3-co-ordinated), which is expected to lead to a substantial increase in the reorganization energy, λ. Moreover, as noted in the Introduction, the change in geometry also gives rise to a large increase in E_0 to 670 mV. The effect of the changes in λ and E_0 on the rate of ET depends on the extent to which the changes in these two parameters compensate. Obtaining an estimate of the change in λ requires extensive quantum mechanical analyses, which is beyond the scope of the present study. The conclusion that can be drawn from the experiments at this stage is that the effects on λ and E_0 to a large extent apparently compensate, in view of the relatively modest difference in ET rates between the two protein variants.

Cu-H117G exhibits a lower k_2 than WT azurin with 5-dRf as the reductant. The difference in midpoint potential cannot be invoked as a possible cause for the difference in rates. In the absence of external ligands, the Cu-H117G midpoint potential amounts to 670 mV [21]. The driving force for the ET reaction from 5-dRf to Cu-H117G should be much larger than for WT azurin, therefore. Two other factors may play a role. In WT and Im-Cu-H117G azurin, the pathway for ET runs through an imidazole moiety that is directly co-ordinated to the Cu [21,39,40]. For Cu-H117G, on the other hand, it runs through one or more loosely organized water molecules [16,17]. The donor–acceptor electronic coupling in the latter case may be expected to be much lower than in the other two proteins. Second, the network of water molecules that fill the gap in the Cu co-ordination shell of the H117G protein will need to adopt a particular configuration to allow efficient ET. This contributes to the free energy of activation and thereby to the reorganization energy. This

requirement is absent in the case where the gap is filled with an imidazole moiety and where the protein framework holds the imidazole in the proper configuration to facilitate ET. Again, in view of the moderate decrease in activity of the Cu-H117G azurin variant in comparison with WT azurin, the changes in λ, E_0 and donor–acceptor coupling must have compensatory effects on the rate of ET.

IPAR-Cu-H117G exhibits a higher k_2 than WT azurin with IPAR as the reductant, similar to Im-Cu-H117G. It is conceivable that the flavin moiety of the IPAR that is bound to the H117G represents the place where the electron enters during the ET reaction and that the IPAR functions as an 'antenna' to accept the electron from the $IPAR^{\bullet-}$ radical. Apparently, it is the imidazole moiety that has a decisive influence on the rate. When present as a ligand (Im-Cu-H117G, IPAR-Cu-H177G) the rate is 2.5- to four-fold higher than its absence (Cu-H117G).

It is of interest to contrast the present findings with what has been found for cytochrome c_{550}. Making an active site more accessible does not always need to have the same effect on the protein's activity. Cytochrome c_{550} is an ET protein, similar to azurin, although it also exhibits a small peroxidase activity. Opening up the cavity around the haem group results in a markedly enhanced peroxidase activity [41]. Thus, we see here that increasing the accessibility of a catalytic site enhances catalytic activity, whereas opening up the active site in an electron transfer protein diminishes it.

One of the reasons to synthesize IPAR and use it in laser flash photolysis experiments with H117G azurin was that it might fulfill a dual role: the imidazole moiety could insert into the gap created by the H117G mutation in the Cu co-ordination shell and thereby restore the ET properties of the WT azurin, whereas the riboflavin moiety could act as a strong reductant either by direct photoinduced electron transfer or as an electron donor after extraction of an electron from the Mes buffer. This would allow the study of the electron transfer along the linker connecting the flavin with the Cu site. In both cases, a fast transient is expected in the early stages of the optical response after flash photolysis. Within the time resolution of the experimental set-up (50 μs), no evidence for such a transient could be found. If intramolecular electron transfer has occurred, indeed, its rate must be faster than $k_{et}^{intra} \gg 2 \times 10^4\ s^{-1}$.

Crystal structure of Cu-H117G azurin

The structure reported in the present study is the first oxidized structure of copper-containing H117G azurin. Other attempts to crystallize this mutant have resulted in the crystal structures of a modified form of apo-H117G, largely rearranged as a result of oxidation of the copper ligand Cys112 [42], as well as of a zinc-replaced homodimer [43]. Other, more indirect, evidence for the atomic structure of the copper site was also available and is discussed with reference to the structure reported in the present study.

It is not unexpected that the overall structure of the molecule is largely the same as of WT azurin, given that His117 is positioned on the loop out of the main β-sandwich body of the protein. The loop Cys112-Met121 is reasonably flexible in the absence of the His117 'anchor', yet retains a comparable structure as deduced from relatively low RMS differences upon superposition. There has been much discussion on the nature and geometry of the H117G site, focusing on the remaining ligands and the possibility of co-ordinated water molecules [16,17,21]. Although, in this structure, the three remaining ligands His46, Cys112 and Met121 remain bound to the copper, the site appears to possess a less rigid structure, showing more variability in ligand bond lengths than the WT species, especially in the Cu-S(Met) distances (width of bond length distribution: 0.31 versus 0.12 Å) and Cu-S(Cys) distances (width of bond length distribution: 0.15 versus 0.08 Å) (Table 2). This may support the mix of type 1 tetrahedral and type 2 tetragonal geometries inferred from a Resonance Raman study on the water-bound Cu-H117G species [18].

This variability also extends to the water occupancy of the site, where between zero and two molecules of water were found in the channel created by the H117G mutation within 4.5 Å of the copper. This, together with the high B factors of these water molecules, may naturally be explained by the short residency times of the waters, diffusing in and out of the cavity, which can maximally accommodate two water molecules (as in monomer B). An NMR dispersion study that optimally fitted two water molecules within 3 Å of the copper [16] was performed at low temperature (5 °C), which may lock the molecule and the waters into a particular conformation; similarly an extended X-ray absorption fine structure study (performed at 20 K) indicated an $S(N/O)_3$ ligand set as being most likely for this species [17].

With respect to the electron-transfer characteristics of the H117G mutant, given its structure, the electronic interaction between the (flavin) electron donor and the (azurin) acceptor is crucial in determining k_{et}, where the histidine side chain, missing in Cu-H117G azurin, may play a vital role in ensuring good coupling between the partners. The fact that Im-Cu-H117G

azurin is more readily reduced than WT azurin may point to additional flexibility and/or mobility in the free imidazole group and mutated loop, which may improve the coupling. In the absence of any imidazole-like ligand, as for the Cu-H117G species, k_{et} is expected to be orders of magnitude lower when the cavity would be a vacuum. However, the structure of this species shows up to two loosely bound waters in the co-ordination sphere of the copper site. They clearly may act as conductors for electron transfer bridging the approximately 7 Å gap between the copper and the surface of the protein, as seen in Fig. 10. It leads to observed rates which are lower, although still within the same order of magnitude, than those for WT and Im-Cu-H117G azurin. It is likely that the changed ligand arrangement of the Cu-H117G species also affects the reorganization energy for the reaction, which may contribute to its lower reduction rate when compared to WT and Im-Cu-H117G azurin.

Conclusions

The use of laser flash photolysis and two different flavins (5-dRf and IPAR) as reductants allowed us to probe the reactivity of WT azurin, and the Cu-H117G and Im-Cu-H117G azurin variants. IPAR appeared between ten- and 100-fold less efficient as an electron donor compared to 5-dRf, which was ascribed to the higher midpoint potential of the IPAR ox/semiquinone couple compared to 5-dRf. The imidazole-reconstituted form of H117G azurin behaved similar to WT azurin with respect to reduction by flavins, whereas the Cu-H117G azurin that has a more exposed copper site was less reactive than the two other forms. It is likely that the histidine side chain plays a vital role in ensuring good electronic coupling to the copper site, as well as in minimizing the reorganizational energy associated with the reduction of copper in azurin. A less rigid and more variable copper site is demonstrated by the crystal structure of the Cu-H117G species, with variation both in Cu-ligand bond length and water occupancy of the cavity brought about by the mutation. Despite the increased accessibility to the copper, the more heterogeneous copper site may exhibit decreased electronic coupling, leading to lower electron transfer rates.

Materials and methods

General procedures

Optical absorption spectra were measured with a Perkin-Elmer Lambda 800 UV-visible spectrometer (Perkin Elmer, Waltham, MA, USA). 1H-NMR spectra were recorded on Bruker AC200 (200 MHz) and DMX-600 (600 MHz) spectrometers (Bruker, Ettlingen, Germany). Mass spectra were measured on a Finnigan MAT TSQ-70 spectrometer (Scientific Instrument Services, Ringoes, New Jersey, 08551-1054, USA) with an electrospray interface.

Materials

All reagents for synthesis were obtained from commercial sources and used as received. 5-dRf was a kind gift from Dr Carlo van Mierlo at Wageningen University (the Netherlands). WT and H117G azurin from *P. aeruginosa* were expressed heterologously in *Escherichia coli* strain JM109, and purified according to previously described protocols [15,44]. H117G azurin was isolated in its apo form, and reconstituted just before use with copper and, when applicable, with imidazole, by a 30 min incubation on ice with 1.1 equivalents each of $Cu(NO_3)_2$ and imidazole. Extinction coefficients used [17] were: apo-H117G azurin ε_{280} = 9.1 $mM^{-1}\cdot cm^{-1}$; Cu-H117G azurin ε_{420} = 2.35 $mM^{-1}\cdot cm^{-1}$, ε_{628} = 1.25 $mM^{-1}\cdot cm^{-1}$; Im-Cu-H117G azurin ε_{628} = 5.3 $mM^{-1}\cdot cm^{-1}$. All experiments were performed in 20 mM Mes buffer (pH 6.0).

IPAR synthesis

The synthesis of IPAR is schematically presented in Fig. 2, and is based on the synthesis of 8α-*N*-imidazolyl-riboflavin [26] but with significant modifications of steps (iii) and (iv).

Peracetylation of riboflavin

Riboflavin (5 g, 13.3 mmol) was dissolved in acetic acid (150 mL) and acetic anhydride (150 mL) followed by the addition of perchloric acid (4 mL, 70%). After the addition of water (1 L), the flavin was extracted with dicholoromethane (3 × 50 mL). The organic phase was dried over $MgSO_4$, filtered and reduced to a volume of 30 mL by rotary evaporation. The flavin was then precipitated by adding cold dry diethyl ether (3 × 200 mL) and dried protected from light in a dessicator over P_2O_5. Yield 80% (10.5 g), M_r = 544. ^{1}H-NMR (200 MHz, $CDCl_3$): δ (ppm) 1.67 (2′-$OCOCH_3$); 2.08 (5′-$OCOCH_3$); 2.22 (3′-$OCOCH_3$); 2.28 (4′-$OCOCH_3$); 2.44 (8α-CH_3); 2.57 (8α-CH_3); 4.21, 4.23, 4.27, 4.29, 4.40, 4.42, 4.47, 4.48 (5′-CH_2); 4.93, 5.12 (1′-CH_2); 5.44 (3′-CH_2, 4′-CH_2); 5.66 (2′-CH_2); 7.56 (9-CH); 8.03 (6-CH); 8.57 (3-NH).

8α-monobromination of tetraacetyl riboflavin

Tetraacetyl riboflavin (7 g, 13 mmol) was dissolved in boiling dioxane (70 mL) and dibenzoperoxide (60 mg) was added. Bromine (2.9 g) diluted in dichloromethane (10 mL) was then added dropwise to the mixture, followed by

30 min of refluxing. The mixture was concentrated to dryness *in vacuo*. The oily residue was redissolved in dichloromethane (70 mL), washed with 100 mM phosphate buffer (pH 7.0) (2 × 50 mL) and once with Milli-Q water (Millipore, Billerica, MA, USA) (50 mL). The organic layer was dried over $MgSO_4$, filtered and reduced to 30 mL by evaporation. The flavin was precipitated by addition to dry cold diethyl ether (2 × 200 mL) and dried protected from light in a dessicator over P_2O_5. Yield 80% (10.3 g), M_r = 623. ^{1}H-NMR (200 MHz in $CDCl_3$): as tetratacetyl-riboflavin but with the following differences: δ (ppm) 2.44 (8α-CH_3) absent; 4.68 (8α-CH_2); 7.82 (9-CH); 8.09 (6-CH); 8.84 (3-NH).

Substitution of 8α-bromo-tetraacetyl-riboflavin with 1-(3-aminopropyl)-imidazole

8α-bromo-tetraacetyl-riboflavin (2 g, 3.0 mmol) was dissolved in dimethyl formamide (4 mL) and cooled on ice. Aminopropyl imidazole (0.4 g, 3.2 mmol) diluted in dimethyl formamide (4 mL) was slowly added at 4 °C to the flavin mixture over 45 min, followed by 1 h of incubation on ice when light protected. The flavin was precipitated with cold dry diethyl ether (100 mL), and dried protected from light *in vacuo*. The product was then purified by silica gel column chromatography (eluent: dicholoromethane/methanol 90 : 10 to 85 : 15, v/v). The appropriate fractions were pooled, concentrated, dried over $MgSO_4$, filtered and precipitated again with diethyl ether as above. Yield 10% (0.23 g), M_r = 667. ^{1}H-NMR (600 MHz): δ (ppm) 1.802, 2.081, 2.145, 2.281 (2′, 3′, 4′, 5′-$OCOCH_3$); 2.120 (8δ-CH_2); 2.469 (7α-CH_3); 2.770, 2.781, 2.789, 2.800, 2.812, 2.822, 2.831, 2.842, 2.851 (8γ-CH_2); 3.908, 3.934, 3.990, 4.016 (8α-CH_2); 4.124, 4.135, 4.146 (8ε-CH_2); 4.237, 4.246, 4.258, 4.266, 4.426, 4.442, 4.463, 4.467 (5′-CH_2); 4.860 (1′-CH_2); 5.410 (3′,4′-CH); 5.545, 5.618, 5.675 (2′-CH_2); 6.952 (5-CH imidazole); 7.070 (4-CH imidazole); 7.533 (2-CH imidazole); 7.808 (9-CH); 8.035 (6-CH). ^{1}H -NMR and ^{13}C-NMR spectra were recorded in D_2O using 2D-GS COSY, HMQC-GS ^{13}C H COSY, ^{13}C HMBC nodec (long-range CH COSY). The resulting assignment is: ^{13}C-NMR (600 MHz) δ (ppm): 18.4 (7α-CH_3); 20.3, 20.6, 20.8, 21.0 (2′, 3′, 4′, 5′-OC-OCH_3); 31.0 (8δ-CH_2); 44.7 (8ε-CH_2); 46.5 (8γ-CH_2); 51.4 (8α-CH_2); 61.8 (5′-CH_2); 68.7 (3′-CH_2); 70.6 (4′-CH_2), (1′, 2′-CH_2 are not detected); 113.0 (9-CH); 118.7 (5-CH imidazole); 130.9 (4-CH imidazole); 133.1 (6-CH); 138 (2-CH imidazole); 134.5, 135.7, 136.0, 155.0, 170.2, 170.7 (carbons and carbonyls from the riboflavin ring).

Deacetylation of the ribityl side chain

The product (30 mg) was dissolved in 0.9 mL of dry methanol. Potassium butanolate (60 mM; 0.3 mL) was added dropwise to the flavin in the dark. After stirring for 150 min, the reaction was stopped by adjusting the pH to 6.0 by the addition of 15% acetic acid. Milli-Q water was added to give a final volume of 15 mL. This mixture was purified by preparative reverse phase HPLC using a Biocad control system (Applied Biosystems, Foster City, CA, USA) with an Alltima RP18-5 μ 10 × 250 mm column (Alltech, Lokeren, Belgium) (eluent: 1% trifluoroacetate, 5–10% acetonitrile). Yield 30% (10 mg), M_r = 499.

Extinction coefficient of IPAR

The extinction coefficient of IPAR at 445 nm, ε_{445}, was determined using a ^{1}H-NMR spectrum of a stock of IPAR in D_2O containing 100 μM trimethylsilylpropionate. Peaks corresponding to known protons in IPAR were integrated and calibrated against the integrated area of the trimethylsilylpropionate peak to obtain the IPAR concentration. Visible absorption spectra of several dilutions of the IPAR sample were measured, and the ε_{445} derived by correlating A_{445} with the concentration of IPAR.

Affinity of IPAR for Cu-H117G azurin

A concentrated stock of H117G apoazurin was first reconstituted by incubation with 0.8 equivalents of $Cu(NO_3)_2$ at 4 °C for 1 h. This protein stock was diluted by addition to an anaerobic cuvette containing 2 mL of deoxygenated 20 mM Mes (pH 6.0) to a final concentration of approximately 50 μM. Aliquots from a 10 mM stock of IPAR were then added to the protein and allowed to equilibrate before recording optical spectra in range 520–800 nm, where the recovery of the blue colour of the imidazole-reconstituted type-I site is observed. Because only IPAR with a deprotonated imidazolyl moiety can bind Cu-H117G azurin, the binding reaction $Cu-H117G + IPAR \rightleftarrows IPAR-Cu-H117G$ (dissociation constant K_d) is in competition with the protonation/deprotonation equilibrium $IPAR + H^+ \rightleftarrows IPAR-H^+$(dissociation constant K_a), analogous to binding of imidazole to Cu-H117G azurin [17]. Similarly, the increase in A_{628} upon the addition of IPAR is dependent on K_d^{app}, the apparent dissociation constant, as given by the equations:

$$(L.Az)^2 - (Az_t + L_t + K_d^{app}) \cdot (L.Az) + Az_t \cdot L_t = 0 \quad (1)$$

$$A_{628} = \varepsilon_{628}^{nl} Az + \varepsilon_{628}^{IPAR} L.Az \quad (2)$$

$$Az_t = Az + L.Az \quad (3)$$

Az_t and L_t represent the total concentrations of Cu-H117G azurin and IPAR in the solution, respectively; Az and $L.Az$ are the concentrations of free Cu-H117G and IPAR-bound Cu-H117G azurin, respectively; A_{628} is the absorption of the sample at 628 nm; and ε_{628}^{nl} and ε_{628}^{IPAR} are the extinction coefficients at 628 nm for the Cu-H117G and IPAR-Cu-H117G species respectively.

The value K_d^{app} obtained by fitting the data to Eqns (1–3) can then be used to obtain the true dissociation constant, K_d, by taking into account the pK_a of the IPAR imidazolyl group (7.0 at 25 °C) [45] and by applying [21]:

$$K_d^{app} = K_d \cdot (1 + \alpha) \quad (4)$$

$$\log \alpha = pK_a - pH \quad (5)$$

Redox potentiometry of IPAR

Potentiometric titrations of IPAR were performed at 25 °C in a 10 mL anaerobic cuvette [46]. Argon was bubbled through a solution of 20 mM of Mes at pH 6.0 for 1 h, before adding IPAR with a Hamilton syringe via a rubber septum to give a final concentration of approximately 30 μM. The head space above the solution was flushed with argon throughout the titration, and the solution was stirred continuously. Sodium dithionite was used as a reductant, and potassium ferricyanide as an oxidant. Enough oxidant or reductant was added to the solution so as to change the potential by between 20 and 40 mV each time, and the solution was allowed to stabilize for 2 min before recording the optical absorbance spectrum. Solution potentials were measured by using a gold electrode connected to a Schott CG 825 potentiometer (SI Analytics, Mainz, Germany), with a saturated calomel electrode as the reference electrode. All potentials reported here are with reference to the NHE electrode. E_1 and E_2 (*vide infra*) could be determined by fitting the absorbance changes to the Nernst equations for the two redox couples sq/hq and ox/sq simultaneously (ox, sq and hq refer to the oxidized, semi-reduced and fully reduced forms of the flavin, respectively) as:

For the two redox couples $sq + e^- \rightleftarrows hq$ and

$$ox + e^- \rightleftarrows sq$$

with

$$\alpha_1 = [hq]/[sq]$$

$$\alpha_2 = [sq]/[ox]$$

and

$$[ox] + [sq] + [hq] = [\text{total IPAR}]$$

the solution potential E is dependent on the redox potentials for the two couples:

$$E = E_1 - (RT/F)\ln\alpha_1 \quad (6)$$

$$E = E_2 - (RT/F)\ln\alpha_2 \quad (7)$$

The absorption at 445 nm, A_{445}, changes with solution potential E according to:

$$A_{445}(E) = [ox(E)] \cdot \varepsilon_{445}^{ox} + [sq](E) \cdot \varepsilon_{445}^{sq} + [hq](E) \cdot \varepsilon_{445}^{hq} \quad (8)$$

where ε_{445}^{ox}, ε_{445}^{sq} and ε_{445}^{hq} represent the extinction coefficients of the ox, sq and hq forms of IPAR at 445 nm respectively. Both ε_{445}^{ox} (*vide supra*) and ε_{445}^{hq} (which could be estimated from the end point of the titration) were fixed, leaving only ε_{445}^{sq} to be varied in the fitting procedure.

Laser flash photolysis

Details of the laser flash photolysis apparatus, data collection and analysis were as described previously [47,48]. Briefly, sample photoexcitation was achieved by irradiating the sample with a 337 nm laser-flash (PTI PL-2300 model nitrogen laser, PTI International, Birmingham, New Jersey 08011, USA, flash duration, 0.6 ns). Flash-induced absorbance changes were followed by illuminating the sample with a perpendicular monochromatic light beam at the desired wavelength, with the signal being detected by a photomultiplier, amplified and recorded in a digital oscilloscope. Sample buffer (1 mL) containing 100 μM of either 5-dRf or IPAR in 20 mM Mes (pH 6.0) was sealed into a 3 mL cuvette with a tapered neck using rubber septa, and made anaerobic by vigorous bubbling with argon for 2 h. Aliquots of concentrated solutions of azurin were then added by means of a gas tight Hamilton syringe (Hamilton, Bonaduz, Switzerland), and the sample was kept anaerobic by flushing the head space with argon. All experiments were performed under pseudo-first-order conditions, where the concentration of protein electron acceptor (> 10 μM) exceeded that of the electron donor, either 5-dRfH$^\bullet$ or IPAR, produced per flash (< 1 μM) [34] and the kinetic traces were well fitted to single monoexponential decays.

Crystallization and X-ray data collection

Large single crystals of azurin H117G were obtained by sitting drop vapor diffusion at 293 K, using protein at a concentration of 17 mg·mL^{-1}. Protein solution (1 μL) was mixed with 1 μL of a precipitant solution containing 31% (w/v) of poly(ethylene glycol) 2000 monomethyl ether and 0.1 M Tris/HCl buffer at pH 8.7. This was suspended above a reservoir of 500 μL of the same precipitant solution in a sealed well of a crystallization plate. For data collection, a crystal was transferred into a harvesting buffer containing 34% (w/v) of poly(ethylene glycol) 2000 MME and 0.1 M Tris/HCl at pH 8.7, mounted in a nylon loop and flash-cooled in liquid nitrogen. Diffraction data were collected on beam line BW7A at EMBL/DESY (Hamburg, Germany) and integrated and scaled using the HKL suite [49] and inspected with XPREP (Bruker, Billerica, USA). Azurin H117G crystallized with unit cell constants of a = 47.59 Å, b = 85.88 Å and c = 170.25 Å and angles of α = 90.0°, β = 90.0° and γ = 90.0°, indicating an orthorhombic crystal system. The data scaled well in space group $P\ 2_12_12_1$ with six monomers per asymmetric unit but, during refinement, it became obvious that the correct choice of space group was indeed $P\ 2_1$ with the monoclinic β angle coinciding to 90.0°, the monoclinic axis **b′** being the former **c** axis

and 12 monomers per asymmetric unit. Further reduction of the crystal symmetry to triclinic *P*1 was attempted but did not improve refinement.

With this particular unit cell geometry and the additional relation of $b = 2c$ in the monoclinic cell, several types of twinning disorder were technically possible (Fig. S1B) and the diffraction images and reflection files were analyzed for twinning by pseudo-merohedry [50,51], reticular merohedry [52] and order–disorder twinning [53], although none of these cases applied.

However, refinement of the structure was complicated by the presence of translational pseudosymmetry in the asymmetric unit that gave rise to a pseudo origin peak in the native Patterson map with a height corresponding to 77% of the origin peak at (0, 0, 1/3) (Fig. S1D). Consequently, in the reciprocal lattice, a major part of the intensities of reflections along the reciprocal **l** axis showed a distinct pattern, with only every third reflection being of high intensity (Fig. S1C). This effect can severely complicate structure solution and it is typically described to lead to situations where refinement stalls at high R_{cryst}/R_{free} values, as has been recognized early by Phillips *et al*. [54]. In his discussion of pseudo-translation, Buerger [55] suggested treating such structures as the sum of a superstructure and its complement substructures (i.e. the individual protein monomers). To obtain correct reliability indices in refinement, Gramlich [56] and Böhme [57] proposed separating the reflections into the respective contributions of superstructure and substructure. The separate normalization of two sets of structure factors was overcome in an algorithm proposed subsequently [58], where the procedure was based on the probabilistic theory of phase relationships [59]. Although the theoretical foundations are thus well established, none of the currently available refinement software contains the feature of renormalization of structure factors based on pseudo-translation. Consequently, the presence of translational pseudo-symmetry often hinders structure solution and refinement, unless extensive workarounds are applied [60]. This problem has been recognized by the developers of the refinement suite BUSTER/TNT and will be addressed in forthcoming releases of the software, although the option is not available at the time of writing this manuscript (C. Vonrhein, personal communication).

For the unambiguous identification of copper atoms in the structure, two additional data sets were collected. Wavelengths were chosen directly below (1.3766 Å) and above (1.3837 Å) the K-edge of copper and data were collected to a limiting resolution of 1.8 Å from the same crystal used for high-resolution data collection.

Model building and crystallographic refinement

The structure of azurin H117G was solved by molecular replacement with the co-ordinates of WT azurin from *P. aeruginosa* (PDB code: 4AZU) [14]) using the software PHASER [61]. Six copies of azurin were placed in the asymmetric unit with data processed in space group $P2_12_12_1$, and refinement was carried out using REFMAC [62]. The software COOT [63] was used for several rounds of model building, yielding a final crystallographic *R*-factor of 0.226 and an R_{free} of 0.273 using data to a resolution of 1.35 Å. Both values were very high, such that refinement in a lower symmetry space group, monoclinic $P2_1$, was carried out after re-indexing the data and extending the content of the asymmetric unit to 12 monomers. The loop region surrounding the mutated residue G117 was not fully defined in all monomers, most likely as a result of differences in the crystal packing environment (Fig. S2A). However, in the initial electron densities in space group $P2_12_12_1$, all loops regions were defined. Because the higher symmetry technically corresponds to a partial averaging of electron density of the lower symmetry space group, we inspected the electron density maps for the $P2_1$ refinement after 12-fold noncrystallographic averaging. In this map, the loop region was fully defined and we consequently chose to model all loops after the mean density and subsequently used strong noncrystallographic symmetry restraints during refinement.

Further refinement was carried out with BUSTER/TNT [64] using translation/libration/screw refinement and noncrystallographic symmetry restraints with an anisotropic U_{ij} temperature factor model to yield final R_{cryst}/R_{free}-values of

Table 3. Data collection and refinement statistics for azurin H117G.

Data collection	
Space group	$P2_1$
Resolution range (Å)	100–1.35 (1.45–1.35)[a]
Number of observations	150,789 (26,249)
Completeness (%)	91.9 (88.8)
Multiplicity	2.79 (2.26)
$I/\sigma(I)$	7.6 (2.6)
R_{int}	0.084 (0.377)
$R_{p.i.m.}$	0.046 (0.250)
R_{cryst} (REFMAC)[b]	0.181 (0.234)
R_{free} (REFMAC)[b]	0.238 (0.318)
R_{cryst} (BUSTER/TNT)[c]	0.172 (0.134)
R_{free} (BUSTER/TNT)[c]	0.202 (0.154)
rmsd (BUSTER/TNT)	
Bond lengths (Å)	0.010
Bond angles (°)	1.34
Cruickshank's DPI	0.060
Mean *B* value (Å^2)	24.1

[a] Values in parentheses represent the highest resolution shell. $R_{p.i.m.}$ was calculated as described previously [66]; the diffraction precision index (DPI) was also calculated as described previously [67]. [b] Refinement with REFMAC [62] was carried out with an isotropic *B*-factor model because isotropic refinement of U_{ij} yielded only a slight drop in R_{cryst} without a concomitant drop in R_{free}. [c] Refinement with BUSTER/TNT yielded significantly improved statistics using an anisotropic *B*-factor model.

0.172/0.202. The translational pseudosymmetry in the crystals of azurin H117G thus did not impair structure solution in this case and the resulting electron density maps were of outstanding quality, although it did reflect in the *R*-factor statistics from BUSTER/TNT that show an unusual behavior in that the *R*-values are significantly worse in the lowest resolution shells than in the higher resolution shells (Fig. S1A). Indeed, using a low-resolution cut-off of 8 Å for refinement led to R_{cryst}/R_{free}-values of 0.138/0.155. This can be explained by the pseudosymmetry operation that is not purely translational, such that its effects [65] unfold only at lower resolution (Fig. S3). The problem in refinement hereby lies with the definition of the *R*-factor itself that assumes an approximately equal distribution of atoms within the unit cell. This assumption breaks down in the presence of a dominant translation vector. No remedy for this effect exists but, in particular in this case, the electron density maps were of very high quality and allowed for building of a complete model. Co-ordinates have been deposited in the PDB (PDB code: 3N2J). Data collection and refinement statistics are presented in Table 3.

Acknowledgements

Dr B. Aguilera and Dr A. W. J. W. Tepper are gratefully acknowledged for their assistance with the synthesis and purification of IPAR and the fitting of the redox potentiometric data, respectively. We thank Dr Carlo van Mierlo for the gift of 5-dRf. The assistance of Dr P. van Vliet during the early stages of this work is gratefully acknowlededged. This work was supported in part by research grants from the Spanish Ministry of Science and Innovation (BFU2006-01361), the Andalusian Government (BIO198) and the EU FEDER Program.

References

1 Sokerina EV, Ullmann GM, van Pouderoyen G, Canters GW & Kostic NM (1999) Electrostatic effects on the kinetics of photoinduced electron-transfer reactions of the triplet state of zinc cytochrome c with wild-type and mutant forms of *Pseudomonas aeruginosa* azurin. *J Biol Inorg Chem* **4**, 111–121.

2 van de Velde F, Konemann L, van Rantwijk F & Sheldon RA (2000) The rational design of semisynthetic peroxidases. *Biotechnol Bioeng* **67**, 87–96.

3 Zhou JS & Kostic NM (1992) Photoinduced electron-transfer from zinc cytochrome-C to plastocyanin is gated by surface-diffusion within the metalloprotein complex. *J Am Chem Soc* **114** 3562–3563.

4 Hu YZ, Tsukiji S, Shinkai S, Oishi S & Hamachi I (2000) Construction of artificial photosynthetic reaction centers on a protein surface: vectorial, multistep, and proton-coupled electron transfer for long-lived charge separation. *J Am Chem Soc* **122**, 241–253.

5 Immoos CE, Di Bilio AJ, Cohen MS, Van der Veer W, Gray HB & Farmer PJ (2004) Electron-transfer chemistry of Ru-linker-(heme)-modified myoglobin: rapid intraprotein reduction of a photogenerated porphyrin cation radical. *Inorg Chem* **43**, 3593–3596.

6 Monzani E, Alzuet G, Casella L, Redaelli C, Bassani C, Sanangelantoni AM, Gullotti M, De Gioia L, Santagostini L & Chillemi F (2000) Properties and reactivity of myoglobin reconstituted with chemically modified protohemin complexes. *Biochemistry* **39**, 9571–9582.

7 Shumyantseva VV, Bulko TV, Bachmann TT, Bilitewski U, Schmid RD & Archakov AI (2000) Electrochemical reduction of flavocytochromes 2B4 and 1A2 and their catalytic activity. *Arch Biochem Biophys* **377**, 43–48.

8 De Francesco R, Tollin G & Edmondson DE (1987) Influence of 8-alpha-imidazole substitution of the Fmn cofactor on the rate of electron-transfer from the neutral semiquinones of 2 flavodoxins to cytochrome-C. *Biochemistry* **26**, 5036–5042.

9 Katz E, Riklin A, Heleg-Shabtai V, Willner I & Buckmann AF (1999) Glucose oxidase electrodes via reconstitution of the apo-enzyme: tailoring of novel glucose biosensors. *Anal Chim Acta* **385**, 45–58.

10 Ludwig ML, Schopfer LM, Metzger AL, Pattridge KA & Massey V (1990) Structure and oxidation reduction behavior of 1-deaza-fmn flavodoxins – modulation of redox potentials in flavodoxins. *Biochemistry* **29**, 10364–10375.

11 Silkstone G, Stanway G, Brzezinski P & Wilson MT (2002) Production and characterisation of Met80X mutants of yeast iso-1-cytochrome c: spectral, photochemical and binding studies on the ferrous derivatives. *Biophys Chem* **98**, 65–77.

12 Hamachi I, Tanaka S, Tsukiji S, Shinkai S & Oishi S (1998) Design and semisynthesis of photoactive myoglobin bearing ruthenium tris(2,2′-bipyridine) using cofactor-reconstitution. *Inorg Chem* **37**, 4380–4388.

13 Adman ET & Jensen LH (1981) Structural features of azurin at 2.7 A-resolution. *Isr J Chem* **21**, 8–12.

14 Nar H, Messerschmidt A, Huber R, Vandekamp M & Canters GW (1991) Crystal-structure analysis of oxidized *Pseudomonas aeruginosa* azurin at Ph 5.5 and Ph 9.0 – A pH-induced conformational transition involves a peptide-bond flip. *J Mol Biol* **221**, 765–772.

15 den Blaauwen T & Canters GW (1993) Creation of type-1 and type-2 copper sites by addition of exogenous ligands to the *Pseudomonas aeruginosa* azurin His117Gly mutant. *J Am Chem Soc* **115**, 1121–1129.

16 Kroes SJ, Salgado J, Parigi G, Luchinat C & Canters GW (1996) Electron relaxation and solvent accessibility of the metal site in wild-type and mutated azurins as

determined from nuclear magnetic relaxation dispersion experiments. *J Biol Inorg Chem* **1**, 551–559.
17 Jeuken LJC, Ubbink M, Bitter JH, van Vliet P, Meyer-Klaucke W & Canters GW (2000) The structural role of the copper-coordinating and surface-exposed histidine residue in the blue copper protein azurin. *J Mol Biol* **299**, 737–755.
18 den Blaauwen T, Hoitink CWG, Canters GW, Han J, Loehr TM & Sandersloehr J (1993) Resonance Raman-spectroscopy of the azurin His117Gly mutant – interconversion of type-1 and type-2 copper sites through exogenous ligands. *Biochemistry* **32**, 12455–12464.
19 Sato K, Li C, Salard I, Thompson AJ, Banfield MJ & Dennison C (2009) Metal-binding loop length and not sequence dictates structure. *Proc Natl Acad Sci USA* **106**, 5616–5621.
20 Marshall NM, Garner DK, Wilson TD, Gao YG, Robinson H, Nilges MJ & Lu Y (2009) Rationally tuning the reduction potential of a single cupredoxin beyond the natural range. *Nature* **462**, 113–U127.
21 Jeuken LJC, van Vliet P, Verbeet MP, Camba R, Mcevoy JP, Armstrong FA & Canters GW (2000) Role of the surface-exposed and copper-coordinating histidine in blue copper proteins: the electron-transfer and redox-coupled ligand binding properties of His117Gly azurin. *J Am Chem Soc* **122**, 12186–12194.
22 Lancaster KM, Sproules S, Palmer JH, Richards JH & Gray HB (2010) Outer-sphere effects on reduction potentials of copper sites in proteins: the curious case of high potential type 2 C112D/M121E *Pseudomonas aeruginosa* azurin. *J Am Chem Soc* **132**, 14590–14595.
23 Canters GW, Kolczak U, Armstrong F, Jeuken LJC, Camba R & Sola M (2000) The effect of pH and ligand exchange on the redox properties of blue copper proteins. *Faraday Discuss* **148**, 205–220.
24 Tollin G (1995) Use of flavin photochemistry to probe intraprotein and interprotein electron-transfer mechanisms. *J Bioenerg Biomembr* **27**, 303–309.
25 Blankenhorn G (1976) Nicotinamide-dependent one-electron and 2-electron (flavin) oxidoreduction – thermodynamics, kinetics, and mechanism. *Eur J Biochem* **67**, 67–80.
26 Williamson G & Edmondson DE (1985) Effect of Ph on oxidation-reduction potentials of 8-alpha-N-imidazole-substituted flavins. *Biochemistry* **24**, 7790–7797.
27 Draper RD & Ingraham LL (1968) A potentiometric study of flavin semiquinone equilibrium. *Arch Biochem Biophys* **125**, 802–808.
28 Crowley PB, Matias PM, Khan AR, Roessle M & Svergun DI (2009) Metal-mediated self-assembly of a beta-sandwich protein. *Chemistry: Eur J* **15**, 12672–12680.
29 Walker WH, Singer TP, Hemmeric P and Ghisla S (1972) Studies on succinate dehydrogenase – 8alpha-histidyl-Fad as active center of succinate dehydrogenase. *Eur J Biochem* **26**, 279–289.
30 Edmondson DE & De Francesco R (1991) Structure, synthesis and physical properties of covalently bound flavins and 6- and 8-hydroxyflavins. In *Chemistry and Biochemistry of Flavoenzymes* (Mueller F ed), pp 73–103. Boca Raton, FL, USA.
31 De Francesco R & Edmondson DE (1988) Pka values of the 8-alpha-imidazole substituents in selected flavoenzymes containing 8-alpha-histidylflavins. *Arch Biochem Biophys* **264**, 281–287.
32 Michaelis L & Schubert MP (1938) The theory of reversible two-step oxidation involving free radicals. *Chem Rev* **22**, 437–470.
33 Mayhew SG (1999) The effects of pH and semiquinone formation on the oxidation-reduction potentials of flavin mononucleotide – a reappraisal. *Eur J Biochem* **265**, 698–702.
34 Tollin G, Hurley JK, Hazzard JT & Meyer TE (1993) Use of laser flash-photolysis time-resolved spectrophotometry to investigate interprotein and intraprotein electron-transfer mechanisms. *Biophys Chem* **48**, 259–279.
35 Massey V, Stankovich M & Hemmerich P (1978) Light-mediated reduction of flavoproteins with flavins as catalysts. *Biochemistry* **17**, 1–8.
36 Navarro JA, Delarosa MA & Tollin G (1991) Transient kinetics of flavin-photosensitized oxidation of reduced redox proteins – comparison of C-type cytochromes and plastocyanins. *Eur J Biochem* **199**, 239–243.
37 Moser CC & Dutton PL (1992) Engineering protein-structure for electron-transfer function in photosynthetic reaction centers. *Biochim Biophys Acta* **1101**, 171–176.
38 Gorren ACF, den Blaauwen T, Canters GW, Hopper DJ & Duine JA (1996) The role of His117 in the redox reactions of azurin from *Pseudomonas aeruginosa*. *FEBS Lett* **381**, 140–142.
39 Vandekamp M, Floris R, Hali FC & Canters GW (1990) Site-directed mutagenesis reveals that the hydrophobic patch of azurin mediates electron-transfer. *J Am Chem Soc* **112**, 907–908.
40 Vandekamp M, Silvestrini MC, Brunori M, Vanbeeumen J, Hali FC & Canters GW (1990) Involvement of the hydrophobic patch of azurin in the electron-transfer reactions with cytochrome-C551 and nitrite reductase. *Eur J Biochem* **194**, 109–118.
41 Diederix REM, Ubbink M & Canters GW (2002) Peroxidase activity as a tool for studying the folding of c-type cytochromes. *Biochemistry* **41**, 13067–13077.
42 Hammann C, vanPouderoyen G, Nar H, Ruth FXG, Messerschmidt A, Huber R, Denblaauwen T & Canters GW (1997) Crystal structures of modified Apo-His117Gly and Apo-His46Gly mutants of *Pseudomonas aeruginosa* azurin. *J Mol Biol* **266**, 357–366.
43 de Jongh TE, van Roon AMM, Prudencio M, Ubbink M & Canters GW (2006) Click chemistry with an active

site variant of azurin. *Eur J Inorg Chem* **2006**, 3861–3868.
44 van de Kamp M, Hali FC, Rosato N, Agro AF & Canters GW (1990) Purification and characterization of a nonreconstitutable azurin, obtained by heterologous expression of the *Pseudomonas aeruginosa* Azu gene in *Escherichia coli*. *Biochim Biophys Acta* **1019**, 283–292.
45 Alagaratnam S (2005) *Electron Transfer in Flavodoxin-based Redox Maquettes*. University of Leiden, Leiden, The Netherlands.
46 Dutton PL (1978) Redox potentiometry: determination of midpoint potentials of oxidation-reduction components of biological electron-transfer systems. *Methods Enzymol* **54**, 411–435.
47 Casaus JL, Navarro JA, Hervas M, Lostao A, De la Rosa MA, Gomez-Moreno C, Sancho J & Medina A (2002) Anabaena sp PCC 7119 flavodoxin as electron carrier from photosystem I to ferredoxin-NADP(+) reductase – Role of TRP57 and TYR94. *J Biol Chem* **277**, 22338–22344.
48 Navarro JA, Hervas M, Delacerda B & Delarosa MA (1995) Purification and physicochemical properties of the low-potential cytochrome C(549) from the cyanobacterium *Synechocystis* Sp Pcc-6803. *Arch Biochem Biophys* **318**, 46–52.
49 Otwinowski Z & Minor W (1997) Processing of X-ray diffraction data collected in oscillation mode. *Macromol Crystallogr Pt A* **276**, 307–326.
50 Heitmann D & Einsle O (2008) Pseudo-merohedral twinning in crystals of the dihaem c-type cytochrome DHC2 from *Geobacter sulfurreducens*. *Acta Crystallogr D Biol Crystallogr* **64**, 993–999.
51 Yeates TO (1997) Detecting and overcoming crystal twinning. *Macromol Crystallogr Pt A* **276**, 344–358.
52 Herbst-Irmer R & Sheldrick GM (1998) Refinement of twinned structures with SHELXL97. *Acta Crystallogr B* **54**, 443–449.
53 Dornberger-Schiff K (1956) On Order-Disorder Structures (OD-Structures). *Acta Crystallogr A* **9**, 593–601.
54 Phillips DC, Rogers D & Wilson AJC (1950) Reliability index for centrosymmetric and non-centrosymmetric structures. *Acta Crystallogr A* **3**, 398–399.
55 Buerger MJ (1956) Partial Fourier syntheses and their application to the solution of certain crystal structures. *Proc Natl Acad Sci USA* **42**, 776–781.
56 Gramlich V (1984) The influence of rational dependence on the probability-distribution of structure factors. *Acta Crystallogr A* **40**, 610–616.
57 Böhme R (1982) Direct methods for structures with superstructure effects. *Acta Crystallogr A* **38**, 318–326.
58 Cascarano G, Giacovazzo C & Luic M (1985) Direct methods and superstructures .1. Effects of the pseudo-translations on the reciprocal space. *Acta Crystallogr A* **41**, 544–551.
59 Cascarano G, Giacovazzo C & Luic M (1987) Direct methods and structures showing superstructure effects .2. A probabilistic theory of triplet invariants. *Acta Crystallogr A* **43**, 14–22.
60 Oksanen E, Jaakola VP, Tolonen T, Valkonen K, Akerstrom B, Kalkkinen N, Virtanen V & Goldman A (2006) Reindeer beta-lactoglobulin crystal structure with pseudo-body-centred noncrystallographic symmetry. *Acta Crystallogr D Biol Crystallogr* **62**, 1369–1374.
61 Read RJ (2001) Pushing the boundaries of molecular replacement with maximum likelihood. *Acta Crystallogr D Biol Crystallogr* **57**, 1373–1382.
62 Murshudov GN, Vagin AA & Dodson EJ (1997) Refinement of macromolecular structures by the maximum-likelihood method. *Acta Crystallogr D Biol Crystallogr* **53**, 240–255.
63 Emsley P & Cowtan K (2004) Coot: model-building tools for molecular graphics. *Acta Crystallogr D Biol Crystallogr* **60**, 2126–2132.
64 Blanc E, Roversi P, Vonrhein C, Flensburg C, Lea SM & Bricogne G (2004) Refinement of severely incomplete structures with maximum likelihood in BUSTER-TNT. *Acta Crystallogr D Biol Crystallogr* **60**, 2210–2221.
65 Zwart PH, Grosse-Kunstleve RW, Lebedev AA, Murshudov GN & Adams PD (2008) Surprises and pitfalls arising from (pseudo)symmetry. *Acta Crystallogr D Biol Crystallogr* **64**, 99–107.
66 Weiss MS & Hilgenfeld R (1997) On the use of the merging R factor as a quality indicator for X-ray data. *J Appl Crystallogr* **30**, 203–205.
67 Cruickshank DWJ (1999) Remarks about protein structure precision. *Acta Crystallogr D Biol Crystallogr* **55**, 583–601.

Supporting information

The following supplementary material is available:
Fig. S1. Analysis of azurin H117G data.
Fig. S2. Experimental electron density maps for azurin H117G in particular for the loop region.
Fig. S3. Crystal packing of the twelve azurin monomers in the asymmetric unit of the $P2_1$ cell.

This supplementary material can be found in the online version of this article.

Please note: As a service to our authors and readers, this journal provides supporting information supplied by the authors. Such materials are peer-reviewed and may be re-organized for online delivery, but are not copy-edited or typeset. Technical support issues arising from supporting information (other than missing files) should be addressed to the authors.